Electromagnetic interaction of split-ring resonators: The role of separation and relative orientation

Nils Feth,[1,*] Michael König,[2] Martin Husnik,[3] Kai Stannigel,[2] Jens Niegemann,[2] Kurt Busch,[2] Martin Wegener,[1,3] and Stefan Linden[1,3]

[1] *Institut für Nanotechnologie, Karlsruhe Institute of Technology (KIT), Hermann-von-Helmholtz-Platz 1, D-76344 Eggenstein-Leopoldshafen, Germany*
[2] *Institut für Theoretische Festkörperphysik, Karlsruhe Institute of Technology (KIT), D-76128 Karlsruhe, Germany*
[3] *Institut für Angewandte Physik and DFG-Center for Functional Nanostructures (CFN), Karlsruhe Institute of Technology (KIT), D-76128 Karlsruhe, Germany*
**nils.feth@kit.edu*

Abstract: Extinction cross-section spectra of split-ring-resonator dimers have been measured at near-infrared frequencies with a sensitive spatial modulation technique. The resonance frequency of the dimer's coupled mode as well as its extinction cross-section and its quality factor depend on the relative orientation and separation of the two split-ring resonators. The findings can be interpreted in terms of electric and magnetic dipole-dipole interaction. Numerical calculations based on a Discontinuous Galerkin Time-Domain approach are in good agreement with the experiments and support our physical interpretation.

OCIS codes: (160.3918) Metamaterials; (260.5740) Resonance.

References and links

1. S. Linden, C. Enkrich, M. Wegener, J. F. Zhou, T. Koschny, and C. M. Soukoulis, "Magnetic response of metamaterials at 100 terahertz," Science **306**(5700), 1351–1353 (2004).
2. S. Zhang, W. J. Fan, B. K. Minhas, A. Frauenglass, K. J. Malloy, and S. R. J. Brueck, "Midinfrared resonant magnetic nanostructures exhibiting a negative permeability," Phys. Rev. Lett. **94**(3), 037402–1 (2005).
3. C. Enkrich, M. Wegener, S. Linden, S. Burger, L. Zschiedrich, F. Schmidt, J. F. Zhou, T. Koschny, and C. M. Soukoulis, "Magnetic metamaterials at telecommunication and visible frequencies," Phys. Rev. Lett. **95**(20), 203901–1 (2005).
4. V. M. Shalaev, "Optical negative-index metamaterials," Nat. Photonics **1**(1), 41–48 (2007).
5. C. M. Soukoulis, S. Linden, and M. Wegener, "Physics. Negative Refractive Index at Optical Wavelengths," Science **315**(5808), 47–49 (2007).
6. U. Leonhardt, "Optical conformal mapping," Science **312**(5781), 1777–1780 (2006).
7. J. B. Pendry, D. Schurig, and D. R. Smith, "Controlling electromagnetic fields," Science **312**(5781), 1780–1782 (2006).
8. A. V. Rogacheva, V. A. Fedotov, A. S. Schwanecke, and N. I. Zheludev, "Giant Gyrotropy due to Electromagnetic-Field Coupling in a Bilayered Chiral Structure," Phys. Rev. Lett. **97**(17), 177401–1 (2006).
9. M. Decker, M. W. Klein, M. Wegener, and S. Linden, "Circular dichroism of planar chiral magnetic metamaterials," Opt. Lett. **32**(7), 856–858 (2007).
10. S. Zhang, Y. S. Park, J. Li, X. Lu, W. Zhang, and X. Zhang, "Negative Refractive Index in Chiral Metamaterials," Phys. Rev. Lett. **102**(2), 023901–1 (2009).
11. J. B. Pendry, A. J. Holden, D. J. Robbins, and W. J. Stewart, "Magnetism from conductors and enhanced nonlinear phenomena," IEEE Trans. Microw. Theory Tech. **47**(11), 2075–2084 (1999).
12. N. Liu, H. Guo, L. Fu, S. Kaiser, H. Schweizer, and H. Giessen, "Three-dimensional photonic metamaterials at optical frequencies," Nat. Mater. **7**(1), 31–37 (2008).
13. N. Liu, H. Liu, S. Zhu, and H. Giessen, "Stereometamaterials," Nat. Photonics **3**(3), 157–162 (2009).
14. N. Liu, S. Kaiser, and H. Giessen, "Magnetoinductive and Electroinductive Coupling in Plasmonic Metamaterial Molecules," Adv. Mater. **20**(23), 4521–4525 (2008).
15. M. Decker, S. Linden, and M. Wegener, "Coupling effects in low-symmetry planar split-ring resonator arrays," Opt. Lett. **34**(10), 1579–1581 (2009).
16. I. Sersic, M. Frimmer, E. Verhagen, and A. F. Koenderink, "Electric and Magnetic Dipole Coupling in Near-Infrared Split-Ring Metamaterial Arrays," Phys. Rev. Lett. **103**(21), 213902 (2009).
17. M. C. K. Wiltshire, E. Shamonina, I. R. Young, and L. Solymar, "Dispersion characteristics of magneto-inductive waves: comparison between theory and experiment," Electron. Lett. **39**(2), 215–217 (2003).

#122844 - $15.00 USD Received 15 Jan 2010; revised 23 Feb 2010; accepted 24 Feb 2010; published 15 Mar 2010

18. O. Sydoruk, O. Zhuromskyy, E. Shamonina, and L. Solymar, "Phonon-like dispersion curves of magnetoinductive waves," Appl. Phys. Lett. **87**(7), 072501–1 (2005).
19. G. Dolling, M. Wegener, A. Schädle, S. Burger, and S. Linden, "Observation of magnetization waves in negative-index photonic metamaterials," Appl. Phys. Lett. **89**(23), 231118–1 (2006).
20. M. Decker, S. Burger, S. Linden, and M. Wegener, "Magnetization waves in split-ring-resonator arrays: Evidence for retardation effects," Phys. Rev. B **80**(19), 193102 (2009).
21. W. Rechberger, A. Hohenau, A. Leitner, J. R. Krenn, B. Lamprecht, and F. R. Aussenegg, "Optical Properties of two interacting gold nanoparticles," Opt. Commun. **220**(1-3), 137–141 (2003).
22. K. H. Su, Q. H. Wie, X. Zhang, J. J. Mock, D. R. Smith, and S. Schultz, "Interparticle coupling effects on plasmon resonances of nanogold particles," Nano Lett. **3**(8), 1087–1090 (2003).
23. A. M. Funston, C. Novo, T. J. Davis, and P. Mulvaney, "Plasmon Coupling of Gold Nanorods at Short Distances and in Different Geometries," Nano Lett. **9**(4), 1651–1658 (2009).
24. C. Dahmen, B. Schmidt, and G. von Plessen, "Radiation damping in metal nanoparticle pairs," Nano Lett. **7**(2), 318–322 (2007).
25. P. Olk, J. Renger, M. T. Wenzel, and L. M. Eng, "Distance dependent spectral tuning of two coupled metal nanoparticles," Nano Lett. **8**(4), 1174–1178 (2008).
26. F. Hesmer, E. Tatartschuk, O. Zhuromskyy, A. A. Radkovskaya, M. Shamonin, T. Hao, C. J. Stevens, G. Faulkner, D. J. Edwards, and E. Shamonina, "Coupling mechanisms for split ring resonators: Theory and experiment," Phys. Status Solidi **244**(4), 1170–1175 (2007).
27. A. Arbouet, D. Christofilos, N. Del Fatti, F. Vallée, J. R. Huntzinger, L. Arnaud, P. Billaud, and M. Broyer, "Direct measurement of the single-metal-cluster optical absorption," Phys. Rev. Lett. **93**(12), 127401–1 (2004).
28. O. L. Muskens, N. Del Fatti, F. Vallée, J. R. Huntzinger, P. Billaud, and M. Broyer, "Single-metal nanoparticle absorption spectroscopy and optical characterization," Appl. Phys. Lett. **88**(6), 063109–1 (2006).
29. M. Husnik, M. W. Klein, N. Feth, M. König, J. Niegemann, K. Busch, S. Linden, and M. Wegener, "Absolute Extinction Cross Section of Individual Magnetic Split-Ring Resonators," Nat. Photonics **2**(10), 614–617 (2008).
30. J. S. Hesthaven, and T. Warburton, "Nodal high-order methods on unstructured grids - I. Time-domain solution of Maxwell's equations," J. Comput. Phys. **181**(1), 186–221 (2002).
31. J. Niegemann, M. König, K. Stannigel, and K. Busch, "Higher-order time-domain methods for the analysis of nano-photonic systems," Photon. Nanostruct. - Fundamentals Appl. **7**(1), 2–11 (2009).
32. K. Stannigel, M. König, J. Niegemann, and K. Busch, "Discontinuous Galerkin time-domain computations of metallic nanostructures," Opt. Express **17**(17), 14934–14947 (2009), http://www.opticsinfobase.org/oe/abstract.cfm?URI=oe-17-17-14934.

1. Introduction

The metamaterial concept has enriched optics and photonics with new and fascinating aspects, e.g., magnetism at optical frequencies [1–3], negative index materials [4,5], transformation optics [6,7], and strong chirality [8–10]. In most photonic metamaterials, these phenomena result from a dense arrangement of resonant metallic nanostructures (**"**photonic atoms**"**). For instance, the split-ring resonator (SRR) [11], i.e., a sub-wavelength metallic ring with a small gap, is *the* prototypical magnetic photonic atom. For proper frequency and polarization of the incident light, resonantly enhanced oscillating currents can be excited in the SRR resulting in a strong magnetic dipole moment. In arrays of SRRs, this can give rise to a strong overall magnetic response.

The total electromagnetic field acting on each photonic atom is the superposition of the incident light field and the scattered fields of all other photonic atoms. Thus, the optical properties of the photonic metamaterial are governed by the interplay of two contributions: (i) The optical response of the individual photonic atoms resulting from the direct excitation with the incident light field and (ii) the mutual electromagnetic couplings of the photonic atoms mediated by the scattered fields. The latter can be decomposed into the elementary, i.e., pair-wise, interactions of the photonic atoms, which depend on the relative separation and relative orientation of the two corresponding photonic atoms.

The importance of coupling effects in photonic metamaterials has been demonstrated in several experiments. For example, coupling between stacked layers of SRRs [12,13] or lateral coupling of twisted SRRs [14] results in spectral splitting of the fundamental magnetic mode and lateral coupling in low-symmetry two-dimensional (2D) SRR arrays leads to a modification of the polarization eigenstates [15]. Experiments on arrays of SRRs revealed an influence of the lateral period on the resonance frequency and linewidth of the fundamental magnetic mode [16]. Another manifestation of interaction effects in metamaterials is the formation of magneto-inductive waves observed at microwave [17,18] and near-infrared

#122844 - $15.00 USD Received 15 Jan 2010; revised 23 Feb 2010; accepted 24 Feb 2010; published 15 Mar 2010

frequencies [19,20]. Near-field and far-field coupling effects have also been theoretically predicted and experimentally observed in the context of plasmonic particles [21–25].

In this letter, we experimentally and theoretically investigate the lateral electromagnetic coupling of SRRs. For this purpose, two SRRs forming a dimer can be considered as a model system which can be utilized for systematic studies of the elementary coupling effects in 2D magnetic metamaterials. The uncoupled system corresponds to two infinitely separated SRRs. Thus, the spectrum of a single SRR multiplied by a factor of two can be utilized as a reference. By comparing the extinction cross-section spectrum of the SRR dimer with this reference, we can directly infer the influence of the mutual electromagnetic interaction on the spectral position of the resonance as well as the corresponding quality factor and the peak value of the extinction cross-section. Investigations of the coupling mechanism of two SRRs for a different excitation geometry and for microwave frequencies have been reported in [26]. In our experiments (calculations), the two SRRs are equivalent since they are both driven by an external plane wave. In contrast, in the experiments (calculations) of reference [26], one of the two SRRs is locally excited and the second SRR is only driven by the electromagnetic near-field of the first SRR. This difference in the excitation geometries has profound consequences: In reference [26], the authors observe for all configurations two resonances while we always find (in accordance with the symmetry of our excitation geometry) only one resonance.

2. Sample design, fabrication, and experimental setup

The four different SRR dimer configurations investigated in this letter are shown in Fig. 1 (a). In the side-by-side configuration and the on-top configuration, the two SRRs have the same orientation and the vertical wires and the bottom wires, respectively, are aligned flush. These two configurations are directly related to a usual 2D SRR array and probe the coupling along the two primitive lattice vectors of the array (see red and blue boxes in (a) and (b), respectively). In the gap-to-gap configuration and the back-to-back configuration, the vertical wires are aligned flush and the two gaps and the two bottom wires, respectively, face each other. These configurations have been chosen because we find particularly strong (weak) SRR-SRR coupling for the gap-to-gap (back-to-back) configuration (see below). We vary the separation of the two SRRs between ~30 nm and ~230 nm. These separations are comparable to those of nearest neighbors in typical 2D SRR arrays. SRR dimers with larger separations have not been fabricated since our measurement technique requires that the total extent of the dimer is small compared to the wavelength of the incident light.

The samples have been fabricated by standard electron-beam lithography, electron-beam evaporation of the 25-nm-thick gold film on top of a glass substrate covered with 5 nm indium tin oxide, and subsequent lift-off. The intended studies require the fabrication of high quality samples in which the shape and size of the SRRs in the different dimers is kept constant. Thus, we have taken great care during the lithography process to adjust the dose for each SRR dimer to guarantee minimal geometric deviations. This is exemplified in Fig. 1 (c), which depicts scanning-electron micrographs of a series of SRR dimers for the gap-to-gap configuration and separations ranging from 210 nm to 35 nm. In addition to the individual SRRs and SRR dimers, large gold plates serving as knife-edges (lateral dimensions 20 μm × 20 μm) have been fabricated on the same substrate.

#122844 - $15.00 USD Received 15 Jan 2010; revised 23 Feb 2010; accepted 24 Feb 2010; published 15 Mar 2010

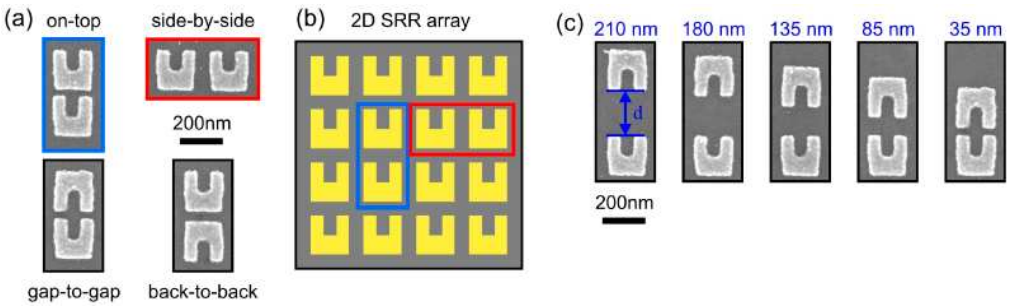

Fig. 1. (a) Scanning-electron micrographs of four different SRR dimers: On-top configuration, side-by-side configuration, gap-to-gap configuration, and back-to-back configuration. (b) Scheme of a usual 2D-periodic square lattice of equally oriented SRRs. The on-top configuration and the side-by-side configuration are directly related to the arrangement of SRRs in a usual 2D array (see red and blue boxes). (c) Scanning-electron micrographs of a series of SRR dimers (gap-to-gap configuration). The separation d between the two SRRs decreases from d = 210 nm (left) to d = 35 nm (right).

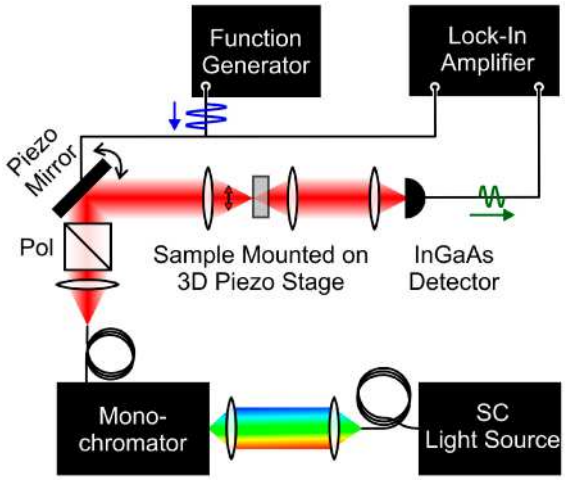

Fig. 2. Scheme of the spatial modulation setup.

The absolute extinction cross-section spectra of individual SRRs and SRR dimers have been measured with a sensitive spatial modulation technique [27,28]. In our setup (see Fig. 2), the output of a white-light laser (Fianium SC450, 2-W average power, 20-MHz repetition frequency) is spectrally filtered by a grating monochromator set to 1 nm resolution. A single-mode optical fiber attached to the output port of the monochromator serves as a spatial filter. The output facette of the optical fiber is imaged onto the sample with a combination of a plano-convex lens (focal length 25 mm) and a 20 × microscope lens (numerical aperture NA = 0.4). Knife-edge measurements reveal a Gaussian beam shape with a typical beam waist r_0 = 1.5 µm for λ = 1200 nm wavelength (250 THz frequency) in the sample plane. A polarizer placed between the two lenses defines the linear polarization of the light impinging on the sample. The transmitted light is collected with a second 20 × microscope lens and detected with a room-temperature InGaAs detector connected to a lock-in amplifier. A piezoelectric tilt mirror mounted in front of the first microscope lens is utilized to periodically modulate the lateral position of the Gaussian beam in the sample plane in one direction with an amplitude of about a = 1.5 µm at a frequency of 4000 Hz. Additionally, we perform a 2D lateral scan (7 µm × 5 µm) of the sample by means of a three-dimensional piezoelectric transducer stage.

#122844 - $15.00 USD Received 15 Jan 2010; revised 23 Feb 2010; accepted 24 Feb 2010; published 15 Mar 2010

The absolute extinction cross-section C_{ext} of a particle for a given frequency is proportional to the maximum of the 2D relative differential signal (RDS) data set RDS_{max} and the effective Gaussian beam area $A = \pi r_0^2/2$:

$$C_{ext} = \frac{A \times RDS_{max}}{\xi}. \quad (1)$$

The proportionality factor $1/\xi$ accounts for the sinusoidal modulation of the beam and depends only on the ratio of the modulation amplitude a and the beam radius r_0 [29].

3. Single SRR

The measured extinction cross-section spectrum of a single SRR for normal incidence and horizontal polarization is depicted by the circles in Fig. 3 (a). The extinction cross-section spectrum exhibits a pronounced resonance at 207 THz frequency with a peak value of C_{ext} = 0.17 μm^2. This resonance can be attributed to the fundamental magnetic mode of the SRR and has been observed both in arrays of SRRs [1,3,12–16] and in isolated SRRs [29]. Basically, the incident electric field excites a resonantly enhanced oscillating current in the SRR. This current induces a magnetic dipole moment oriented perpendicular to the SRR. Additionally, charge accumulations at the ends of the vertical wires of the SRR give rise to an electric dipole moment oriented parallel to the incident light polarization.

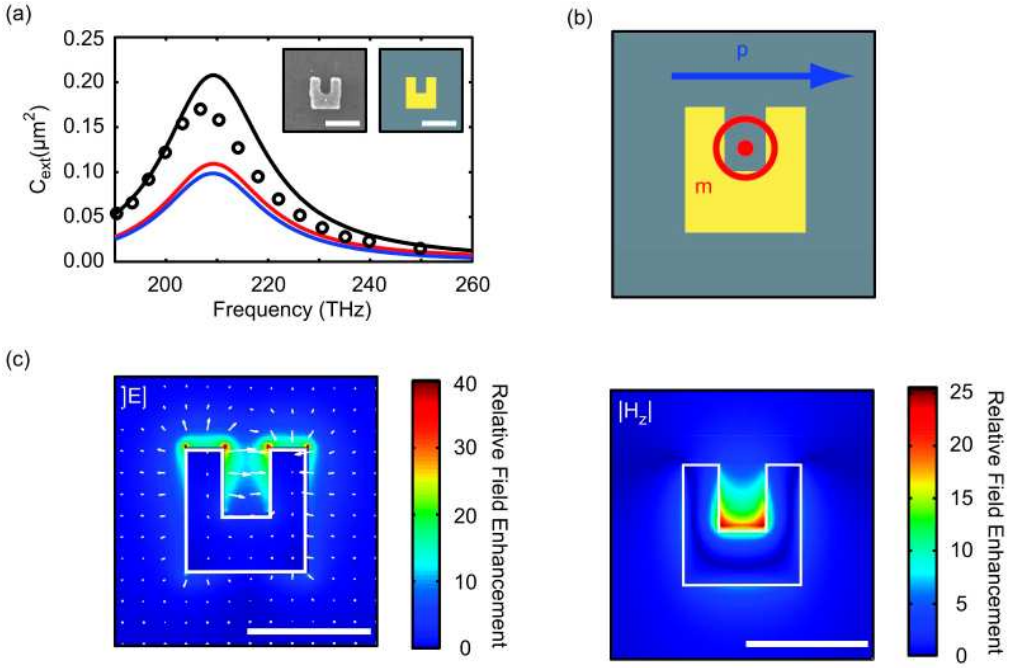

Fig. 3. (a) Measured (circles) and calculated (black curve) extinction cross-section of a single SRR for normal incidence and horizontal polarization. The corresponding calculated absorption cross-section and scattering cross-section spectra are represented by the red and blue curve, respectively. The insets show a scanning electron micrograph of the single SRR and the geometry assumed in our calculations, respectively. The scale bars are 200 nm. (b) Equivalent dipole model for a SRR. The blue (red) arrow corresponds to the electric (magnetic) dipole moment. (c) Calculated electric (left) and magnetic (right) near-field distribution, respectively, for the plane intersecting the middle of the SRR.

The solid black curve in Fig. 3(a) represents the extinction cross-section spectrum of a single SRR calculated with the Discontinuous Galerkin Time-Domain (DGTD) method (see below). The extinction cross-section is given by the sum of the absorption cross-section and the scattering cross-section, i.e., $C_{ext} = C_{abs} + C_{scatt}$. A more detailed analysis of the calculated

#122844 - $15.00 USD Received 15 Jan 2010; revised 23 Feb 2010; accepted 24 Feb 2010; published 15 Mar 2010

data reveals that in the case of our SRR design, C_{abs} and C_{scatt} contribute to approximately equal parts to C_{ext} (compare red and blue curve in Fig. 3(a)). As expected, the resonance disappears for vertical polarization both in the experiment and in the calculations (not shown). A comparison of the extinction cross-section spectra of several nominally identical single SRRs shows that the variation of the resonance frequency is ≤ 5 THz. The corresponding peak values of C_{ext} differ by ≤ 0.005 μm^2.

4. Dipole-dipole interaction model

Before we address the experimental results for SRR dimers, we discuss the anticipated coupling effects in terms of an intuitive dipole-dipole interaction model. In analogy to electric dipole-dipole coupling in plasmonic dimers [21–25], we substitute each SRR by *two* dipoles: (i) an electric dipole oriented parallel to the incident light polarization and (ii) a magnetic dipole oriented perpendicular to the SRR (see Fig. 3(b)). To account for the actual electric and magnetic near-field distribution (see Fig. 3(c)), we position the magnetic dipole in the center of the SRR while the electric dipole is located between the two ends of the SRR. For small separations, i.e., $d \ll \lambda/4$, retardation effects can be neglected. In this case, the interaction between equally oriented dipoles – be it electric or magnetic – yields an increase (decrease) of the resonance frequency for a transverse (longitudinal) arrangement.

Furthermore, coupling of each SRR to the radiation field will be altered by the presence of the second SRR. It acts as an antenna which transfers some of the SRR's electromagnetic near-field to the far-field. This results in an increase of the line width or, equivalently, a decrease of the quality factor of the resonance. However, within this model, exact values of the dimer's quality factors cannot be predicted since it strongly depends on the actual near-field distribution. The increase of the linewidth is related to a decrease of the peak value of C_{ext}. In other words, we expect that the extinction cross-section of the SRR dimer is smaller than the combined extinction cross-section of two uncoupled SRRs.

Due to the antenna effect, we also anticipate that the scattering cross-section becomes more important at the expense of the absorption cross-section for decreasing separation of the two SRRs. For larger separations ($d \geq \lambda/4$), retardation effects become important resulting in periodic modulations of the resonance frequency and the quality factor, respectively, of the dimer's coupled mode [24,25].

The relative strength of the electric dipole-dipole interaction and magnetic dipole-dipole interaction obviously depends on the electromagnetic near-field distribution. Thus, our dipole-dipole model cannot make corresponding *a priori* predictions. However, it allows for intuitive *a posteriori* interpretations of the resulting spectral shifts. For quantitative results, we have to refer to our rigorous numerical calculations (see below).

Finally, we want to emphasize that the dipole-dipole interaction model has to be considered as a first approximation since several aspects of the SRR-SRR interaction cannot be covered within its framework, e.g., the finite extent of the SRRs or coupling of higher order multipoles. Again, these aspects are taken fully into account in our rigorous numerical calculations (see below).

5. SRR dimers

The measured extinction cross-sections for the four dimer configurations are presented in Fig. 4. (a)-(d) as circles. In addition to the spectra of the dimers, we have depicted in each case the spectrum of the same single SRR multiplied by a factor of two as a reference. The solid curves are Lorentzian fits to the experimental data. From these fits, we derive the resonance frequency f_{res}, the peak value of the extinction cross-section spectrum C_{ext}, and the quality factor Q defined as $Q = f_{res} / \Delta f_{res}$, where Δf_{res} is the full width at half maximum of the resonance peak.

#122844 - $15.00 USD Received 15 Jan 2010; revised 23 Feb 2010; accepted 24 Feb 2010; published 15 Mar 2010

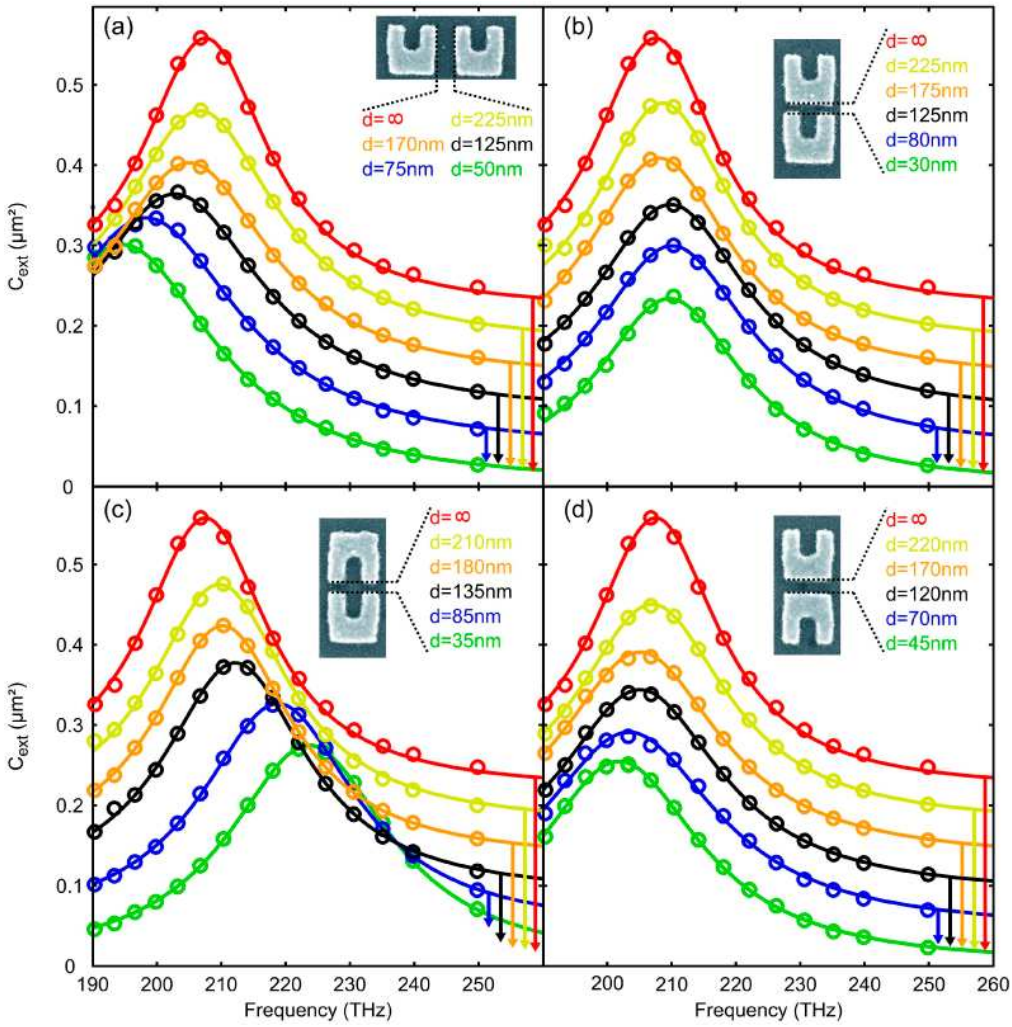

Fig. 4. Measured extinction cross-section spectra of four different sets of SRR dimers for different separations. The symbols correspond to the experimental data. The solid curves are Lorentzian fits to the experimental data. The different curves in each set are vertically displaced for clarity (see arrows). (a) Side-by-side configuration, (b) on-top configuration, (c) gap-to-gap configuration, and (d) back-to-back configuration.

5.1 Side-by-side Configuration

Figure 4(a) depicts the measured extinction cross-section spectra for the side-by-side configuration for separations ranging from d = 50 nm to d = 225 nm. For decreasing separation, the resonance frequency of the dimer's coupled mode gradually shifts to lower frequencies and the corresponding quality factor degrades. Furthermore, we find that the reference's peak value of C_{ext} exceeds that of all dimers in this configuration. For the smallest separation (d = 50 nm), the frequency shift is about 6% of f_{res} of the reference. The quality factor decreases from Q = 8.7 (reference) to Q = 5.5 (d = 50 nm) and the peak value of C_{ext} decreases from C_{ext} = 0.34 μm^2 (reference) to C_{ext} = 0.3 μm^2 (d = 50 nm).

The red shift of the resonance for the side-by-side configuration can be understood in terms of the dipole-dipole interaction model. For symmetry reasons, the incident light field can only excite a symmetric mode of the dimer in which the two electric dipoles and the two magnetic dipoles are oscillating in phase. The electric dipoles are oriented parallel to the axis of the SRR dimer resulting in longitudinal electric dipole-dipole coupling. In contrast, the

#122844 - $15.00 USD Received 15 Jan 2010; revised 23 Feb 2010; accepted 24 Feb 2010; published 15 Mar 2010

magnetic dipoles are oriented perpendicular to the SRR dimer axis, i.e., the magnetic dipoles are coupled transversely. The longitudinal electric dipole-dipole interaction tends to decrease the resonance frequency while the transverse magnetic dipole-dipole interaction has the opposite effect. Thus, the red shift of the resonance suggests that the interaction between the two SRRs is dominated by electric dipole-dipole coupling in case of the side-by-side configuration. The decrease of the quality factor and the peak value of the extinction cross-section is also consistent with the reasoning given above.

5.2 On-Top Configuration

Next, we address the experiments for the on-top configuration. The corresponding extinction cross-section spectra for separations ranging from d = 30 nm to d = 225 nm are depicted in Fig. 4(b). Here, the resonance frequency slightly increases with decreasing separation. The observed spectral shift is comparable to the limits set by the variation of f_{res} due to fabrication tolerances. This small shift is also consistent with the corresponding numerical calculations (see Fig. 5(b)). Additionally, we find a significant reduction of the quality factor and the peak value of the extinction cross-section, respectively. For the smallest separation (d = 30 nm), the quality factor is Q = 7.4 and the peak value of the extinction cross-section is C_{ext} = 0.23 μm^2.

In terms of the dipole-dipole interaction model, one expects a blue shift of the dimers's coupled mode for the on-top configuration since both the electric and the magnetic dipoles are coupled transversely. The weakness of this effect can probably be attributed to additional coupling of higher order multipoles.

The magnitude of the spectral shift of the dimer's resonance frequency with respect to the reference is for small separations a measure for the coupling strength of the two SRRs. A comparison of the results for the side-by-side configuration and the on-top configuration suggests that the nearest neighbor interaction of equally oriented SRRs in dense square arrays is dominated by the side-by side configuration rather than by the on-top. This interpretation is further supported by our numerical calculations (see Fig. 5(a) and (b)).

5.3 Gap-to-Gap Configuration

The measured spectra for the gap-to-gap configuration are shown in Fig. 4(c). Here, the reduction of the separation between the two SRRs leads to a strong increase of the resonance frequency. At the same time, we observe a continuous reduction of Q and C_{ext}. For the smallest separation (d = 35 nm), the shift of the resonance frequency of the dimer's coupled mode is 8% of f_{res} of the reference. The corresponding quality factor is Q = 7.3 and the corresponding peak value of the extinction cross-section is C_{ext} = 0.27 μm^2.

In the gap-to-gap configuration, the two SRRs are rotated against each other by 180° with respect to the interface normal. Again, the incident light field can only couple to a symmetric mode of the dimer. Thus, the two electric dipoles are excited in phase but the two magnetic dipoles are oscillating with a phase shift of π in the gap-to-gap configuration. For transverse dipole-dipole coupling, the interaction of the parallelly oriented electric dipoles increases the resonance frequency while the interaction of the anti-parallelly oriented magnetic dipoles tends to counteract this effect. Again, we find that the interaction between the two SRRs is dominated by electric dipole-dipole coupling.

5.4 Back-to-Back Configuration

Finally, we address the experiments for the back-to-back configuration (see Fig. 4(d)). For this configuration, the reduction of the separation between the two SRRs leads to a slight decrease of the resonance frequency which is comparable to the corresponding spectral shift in the numerical calculations (see Fig. 5(d)). At the same time, we observe a continuous reduction of Q and C_{ext}. For the smallest separation (d = 45 nm), the quality factor is Q = 6.5 and the peak value of the extinction cross-section is C_{ext} = 0.25 μm^2.

Like in the previous case, all dipoles are transversely coupled with the two electric dipoles excited in phase and the two magnetic dipoles oscillating with a π phase shift. However, in

#122844 - $15.00 USD Received 15 Jan 2010; revised 23 Feb 2010; accepted 24 Feb 2010; published 15 Mar 2010

our model, the electric dipoles are further separated in the back-to-back configuration than in the gap-to-gap configuration for the same value of *d*. In contrast, the separation of the magnetic dipoles does not change. Hence, we expect that the relative importance of the electric dipole-dipole interaction becomes weaker. The slight red shift of the resonance even indicates that for the back-to-back configuration the magnetic dipole-dipole coupling is more efficient than the electric dipole-dipole coupling.

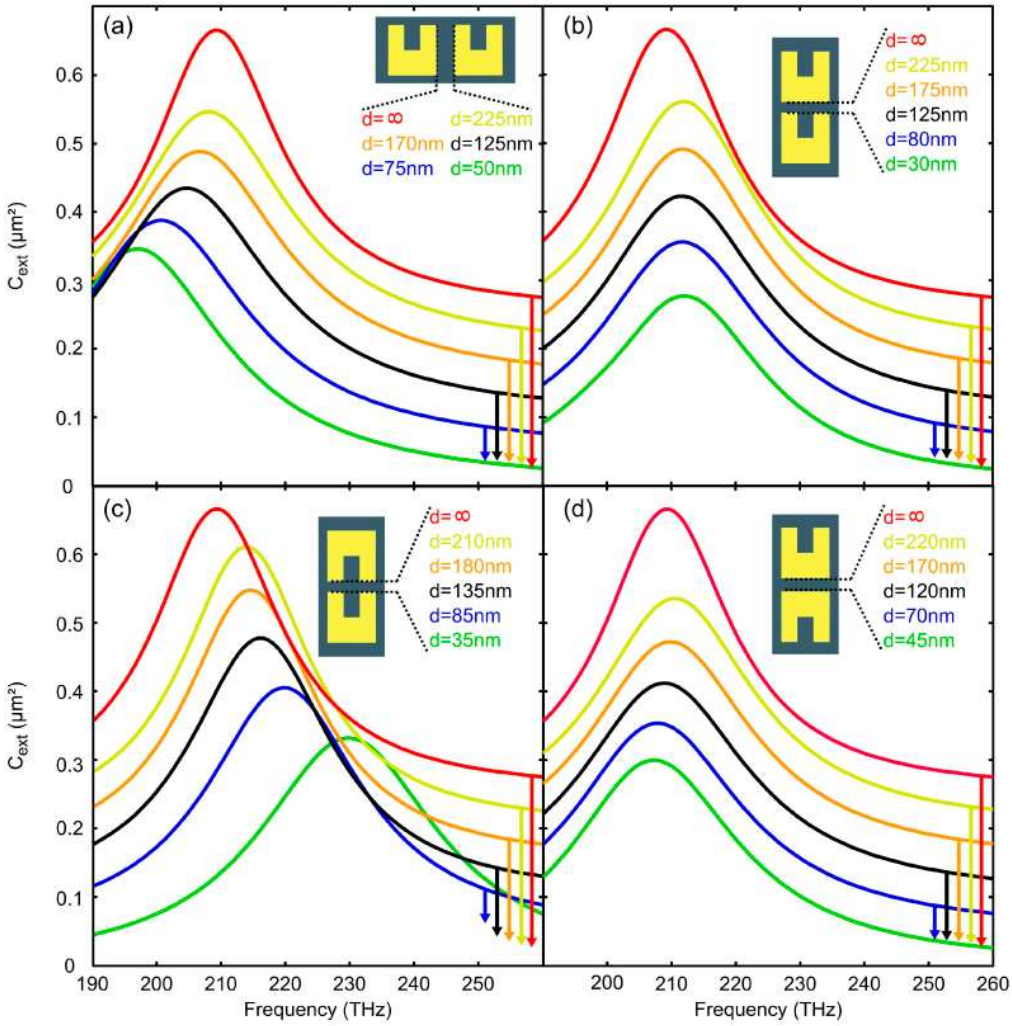

Fig. 5. Calculated extinction cross-section spectra of four different sets of SRR dimers. The geometries and separations of the SRRs correspond to the experiments in Fig. 4. The different curves in each set are vertically displaced for clarity (see arrows). (a) Side-by-side configuration, (b) on-top configuration, (c) gap-to-gap configuration, and (d) back-to-back configuration.

6. Numerical calculations

To support our interpretations, we have performed rigorous numerical calculations based on an in-house DGTD code employing a total-field scattered-field approach and perfectly matched layers [30–32]. The electric permittivity of gold is described with the free-electron Drude model with plasma frequency $\omega_{pl} = 1.378 \times 10^{16}$ s^{-1} and collision frequency $\omega_{coll} = 1.398 \times 10^{14}$ s^{-1}. In all our calculations, the SRRs are characterized by the same set of

#122844 - $15.00 USD Received 15 Jan 2010; revised 23 Feb 2010; accepted 24 Feb 2010; published 15 Mar 2010

geometrical parameters which has been derived from a scanning-electron micrograph of a single SRR (see insets in Fig. 3(a)).

The calculated extinction cross-section spectra of the four configurations are depicted in Fig. 5. Here, the separation matches the corresponding experiment (see Fig. 4) in each case. The numerical calculations qualitatively and almost quantitatively reproduce all trends observed in the corresponding experiments (compare Fig. 4 and Fig. 5).

Additionally, we have calculated extinction cross-section spectra for separations exceeding the experimental range. For separations comparable to or larger than the resonance wavelength, C_{ext} and Q exhibit an oscillatory behavior (not shown). Analogous effects have been observed for plasmonic dimers [24,25]. Furthermore, we find that the DGTD calculations confirm our prediction that the scattering cross-section becomes more important at the expense of the absorption cross-section for the SRR dimer for decreasing separations (not shown).

7. Conclusion

In conclusion, we have experimentally and theoretically investigated the extinction cross-section spectra of SRR dimers. We find that the dimer's resonance frequency shifts with increasing SRR separation. The direction of this shift depends on the orientation of the SRRs in the dimer. The measured (calculated) frequency shift for the gap-to-gap configuration can be as large as 8% (10%) of the resonance frequency of the corresponding single SRR. Even stronger effects are observed with respect to the quality factor of the dimer's coupled mode. Here, we find for the side-by-side configuration a maximum reduction of the quality factor of 37% (30%) compared to the quality factor of a single SRR in our experiments (calculations). Our results imply that the in-plane interaction between SRRs strongly influences the optical properties of two-dimensional metamaterial arrays.

Acknowledgement

We acknowledge support by the Deutsche Forschungsgemeinschaft (DFG) and the State of Baden-Württemberg through the DFG-Center for Functional Nanostructures (CFN) within subprojects A 1.2 and A 1.5. The project PHOME acknowledges the financial support of the Future and Emerging Technologies (FET) programme within the Seventh Framework Programme for Research of the European Commission, under FET-Open grant number 213390. The project METAMAT is supported by the Bundesministerium für Bildung und Forschung (BMBF). The research of S.L. is further supported through a Helmholtz-Hochschul-Nachwuchsgruppe (VH-NG-232). The PhD education of N. F., M. K., and M.H. is embedded in the Karlsruhe School of Optics & Photonics (KSOP). The PhD education of M.K. is further supported by the Studienstiftung des Deutschen Volkes.

#122844 - $15.00 USD Received 15 Jan 2010; revised 23 Feb 2010; accepted 24 Feb 2010; published 15 Mar 2010